IEEE Access
Multidisciplinary | Rapid Review | Open Access Journal

Received April 11, 2021, accepted May 16, 2021, date of publication May 24, 2021, date of current version June 2, 2021.

Digital Object Identifier 10.1109/ACCESS.2021.3083092

Solar Powered Unmanned Aerial Vehicle With Active Output Filter Under Non-Linear Load Conditions

NABIL A. AHMED, (Member, IEEE), AND FAHAD M. ALHUWAISHEL, (Member, IEEE)
Department of Electrical Engineering, College of Technological Studies, The Public Authority for Applied Education and Training, Shuwaikh 70654, Kuwait
Corresponding author: Nabil A. Ahmed (na.ahmed@paaet.edu.kw)

This work was supported by the Public Authority for Applied Education and Training (PAAET) under Project TS-16-09.

ABSTRACT This paper presents a new electric powertrain for solar powered unmanned aerial vehicle (UAV). The proposed system structure is based on the development of the power supply system for both the Solong and Zyphyr aircraft models. The proposed UAV model incorporates the Zyphry UAV use of an AC line feeder instead of DC power lines to power the propellers. The proposed powertrain includes solar panels, an energy management system based on lithium sulfide battery, inverter, AC bus-line and active output filter (AOF). AOF topology is composed of a high switching frequency H-bridge inverter with a reduced size LC filter. The utilization of AOF system reduces the size and weight of the power transmission system and significantly improves its conversion efficiency by introducing an emulated series resistance with the H-bridge stage to ensure high quality pure sinusoidal waveform of the line voltage. This emulated series resistance produces an injected voltage across it to diminish unwanted harmonics created from the non-linear load. A simulation model and experimental setup are created to simulate the proposed system and the system is tested under non-linear load condition with closed-loop feed-back control strategy. The obtained simulation and experimental results demonstrate that high-quality sinusoidal line voltage waveforms can be obtained using the active resistance compensation technique with total harmonic distortion factor less than 3%. Moreover, power losses analysis and conversion efficiency calculation of the proposed system are performed and compared with that of the conventional three-phase PWM inverter, which proved that the power losses are reduced by 31%.

INDEX TERMS Active output filter, active resistance compensation, loss analysis, non-linear load, solar powered, unmanned aerial vehicle.

I. INTRODUCTION

The main goal of using an electric powertrain system operating at a frequency of 400 Hz in aerospace applications instead of conventional low frequency of 50/60 Hz is to reduce the size and weight of the power transmission system [1]. Since conventional passive filters are one of the heaviest elements in power transmission systems due to their lower power intensity compared to the active power components. Therefore, reducing the size and weight of these filters will greatly reduce the size of the power system and thus reduce fuel consumption [2]. The development of the aircraft electric powertrain systems has evolved over the years, passing through many stages until achieving fully developed unmanned aerial vehicle (UAV) technology. The mechanical based speed drives such as constant speed drives (CSD) and integrated engine generator (IDG) is developed to provide mechanical interface with the 400 Hz synchronous alternator [3]–[7]. The mechanical coupling is essentially a variable ratio hydro-mechanical drive that coupled the jet engine shaft to the synchronous alternator through multiple gear stages and hydraulic cylinder block common to both the pump and the motor. However, these mechanical interfaces have numerous disadvantages such as low efficiency, it requires frequent and costly maintenance, large size and weight [8], [9].

Towards more electric aircraft (MEA), the electrical systems have replaced tradition mechanical systems in modern

The associate editor coordinating the review of this manuscript and approving it for publication was Zhixiang Zou.

aircrafts because of their excellent advantages in energy density, high conversion efficiency and requires less maintenance [20]. Therefore, a variable frequency drive (VFD) system has been introduced to eliminate the mechanical interface [10], [11]. However, this involves operating electrical loads over a frequency range. A significant enhancement in both powertrain system size and performance is achieved using variable speed constant frequency (VSCF) powertrain system [12]–[15]. The VSCF powertrain system comprises of a rectifier, a DC-link followed by a PWM inverter with passive (L-C) output filters to generate a sinusoidal load output voltage. The PWM inverter produces the required sinusoidal load voltage at constant frequency. However, VSCF also still has some weaknesses such the limiting switching frequency of PWM inverter in high power applications. Restrictions in the inverter switching frequency leads to a larger size of the elements of the LC output filter with a higher output impedance [16]. The realization of active filters to simulate passive filter components has allowed size reduction for many applications such as realizing passive inductance [17] and an active DC-link for adjustable speed drive systems [18]. It also improves system performance under non-linear load conditions [19].

The persistent progress in the aviation powertrain systems has resulted in a remotely piloted UAV that has been used in a wide range of increasing applications like communications, surveillance, investigations, weather broadcasting, and conducting military operations [21], [22]. However, UAV experiences from numerous difficulties, its continuous need for fossil fuel while flying to supply the combustion engine for aircraft propulsion and low flight endurance, short flight time and low flight endurance [23]. Thus, solar powered UAV has received substantial extent of attention from researchers. A solar-powered UAV utilizes solar energy as a substitute of conventional fossil fuels, converting harvested solar energy into electrical energy to power an electric-propulsion system and other involved apparatus [24]–[27]. The DC-link propulsion system and energy management of the conventional solar powered UAV illustrated in Fig. 1(a) requires an energy storage system such as batteries for night flying or other low solar intensity times. Helios HP01 UAV, proposed by NASA, uses PV panels integrated with lithium ion-based battery pack system to supply 21kW loads of DC propellers [28]. Due to the heavy construction of lithium-ion battery, NASA proposed HELIOS HP03 model that uses hybrid PV and fuel cell power system. This topology has higher energy density and less energy loss compared to the conventional PV battery system. Regrettably, the Helios HP03 crashed after a 30-minute flight, and one of the main causes of this accident was the limited airframe caused by the fuel cell system. In 2005, Solong invented a novel AC drive system which provides a low DC-bus voltage [29]. The effective and lightweight of Solong design enabled it to break its first 48 straight hours of flight record. Subsequently, Zyphyr established PV with a high-power lithium-sulfur battery pack which still maintains the longest aviation endurance record [21].

The inverter in the UAV power system is a crucial part because it handles full power, so any enhancement in the size and efficiency of the inverter will be significantly reflected in the aircraft [10], [20], [25]. Increasing the switching frequency in a PWM classic inverter results in high switching power loss. Conversely, reducing the switching frequency requires bulky passive LC output filters to provide a sinusoidal load output voltage [24]. Challenges to use the active filtration techniques by voltage or current injection have been made since the 1970's to reduce the use of passive filters [30]. In particular, series active filters are capable to suppress voltage harmonics generated by the load or source especially with aggressive deployment in inverter system into electrical vehicles with renewable energy systems [31]–[33]. However, they incorporate large coupling transformer design, and they are weaker in dealing with current harmonics caused by a non-linear load. Fig. 1 shows the development of the power generation system of solar powered UAV. The conventional solar powered UAV with constant DC-bus line to supply the propellers is illustrated in Fig. 1(a). AC-bus line using constant frequency PWM inverter with standard bulky passive L-C filter as a replacement of DC-bus line is shown in Fig. 1(b).

Recently, active output filter (AOF) have been proposed for variable speed constant frequency aircraft system with six-step inverter to eliminate the need of coupling transformer, increasing the conversion efficiency and reduce the overall passive elements sizing in aerospace application [34], [35]. However, only linear loads are considered in these studies.

This paper introduces a new electric powertrain system based on the concept of AOF for solar powered UAV to employ an effective filtration system instead of the use of traditional passive filters. This allows the main inverter that operates at the total rated power to operate at low switching frequency, thus, improves the overall efficiency of the powertrain system. The proposed architecture is a potential improvement to the power supply of both Solong and Zyphyr aircraft models. The proposed UAV model incorporates the Zyphry UAV use of an AC-bus line instead of DC-bus line to power electric motors and loads. The system also includes solar panels and an energy management system based on lithium sulfide batteries, inverter and AOF. The AOF consists of three individual H-bride inverters operating at high frequency and a compact LC power filter. The AOF system is operated at fraction of the rated power of the electrical system, therefore, reduces the size of the power transmission system and significantly improves its conversion efficiency. The system is simulated and tested under non-linear loads using a closed loop control strategy. Active compensation technology is employed to ensure high quality of sinusoidal voltage waveforms at the terminals of the non-linear load. A simulation model is created in Matlab Simulink to simulate the proposed system, and the obtained results proved the efficiency of the system. The results demonstrate that high-quality line voltages are

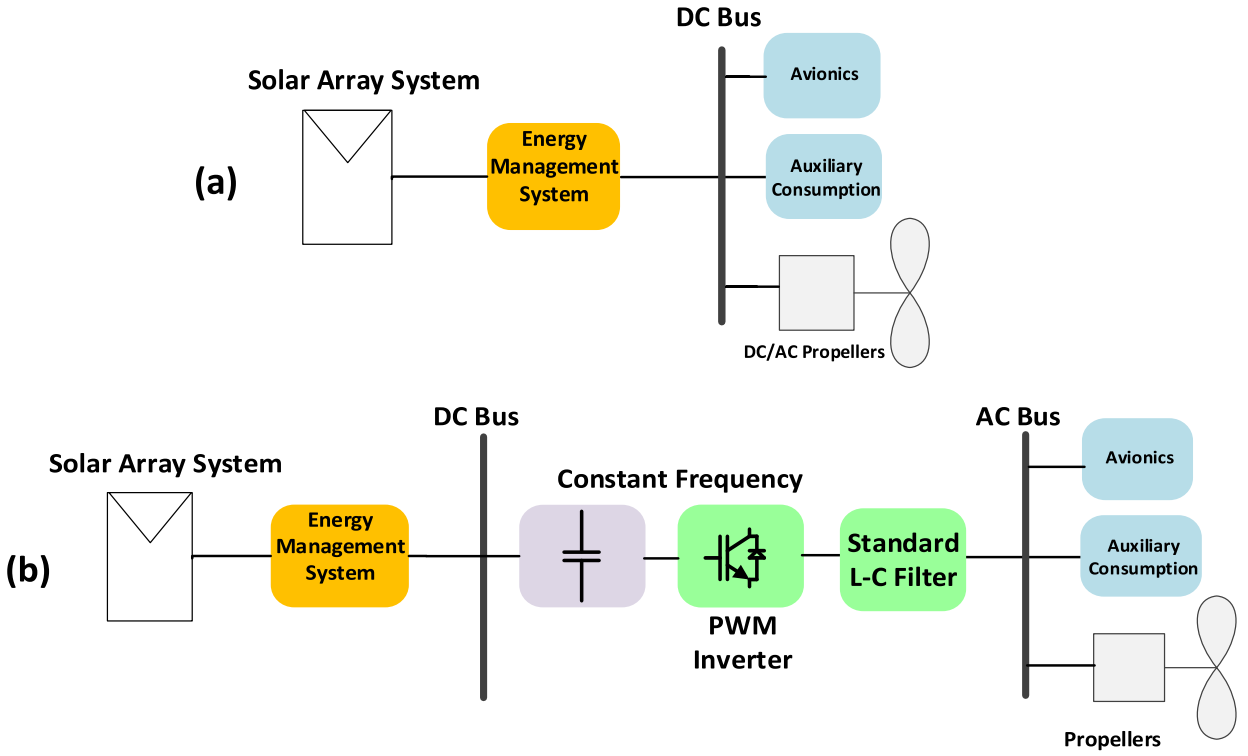

FIGURE 1. Conventional solar powered UAV, (a) Conventional DC bus-line and (b) PWM inverter with standard L-C filter and AC-bus line.

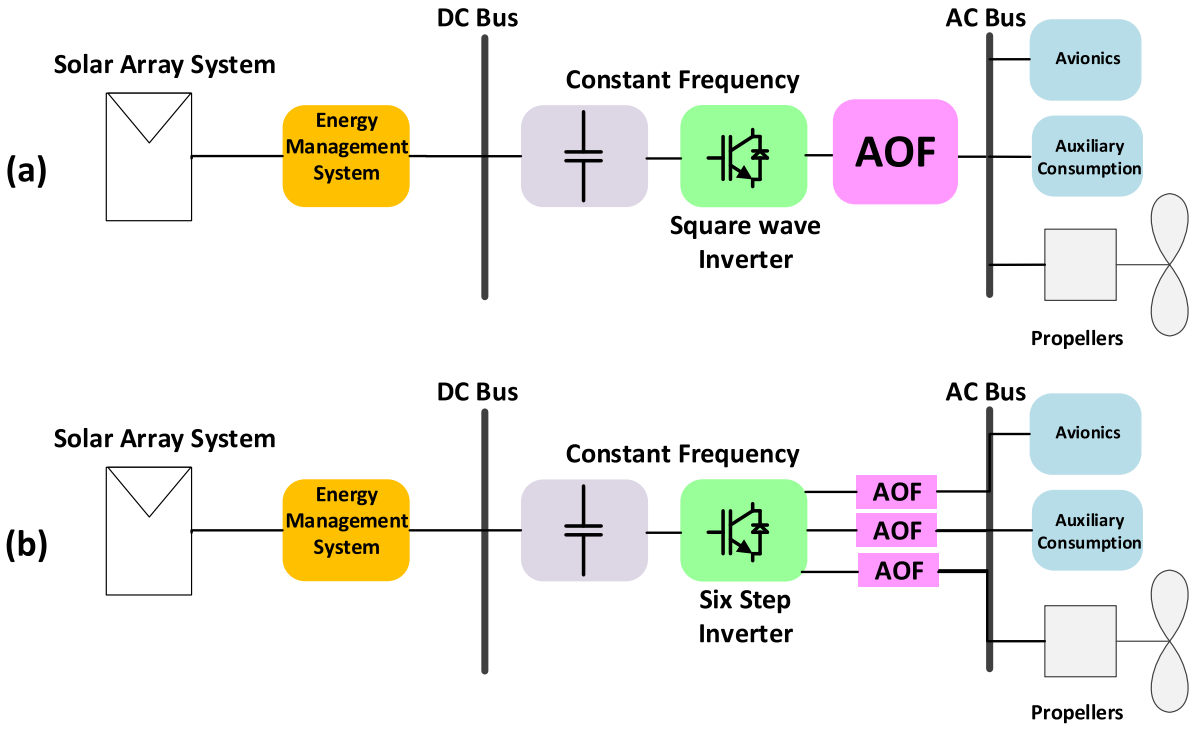

FIGURE 2. Proposed solar powered UAV and AOF, (a) Single-phase square wave inverter with AC-bus line and (b) Three-phase six-step inverter with AC-bus line.

obtained using the active resistance compensation technique with a total harmonic distortion less than 3%. Moreover, power loss analysis and conversion efficiency calculation of the proposed system are performed and compared with that of the conventional three-phase PWM inverter, where the power loss is improved by 31%. Fig. 2(a) shows the schematic

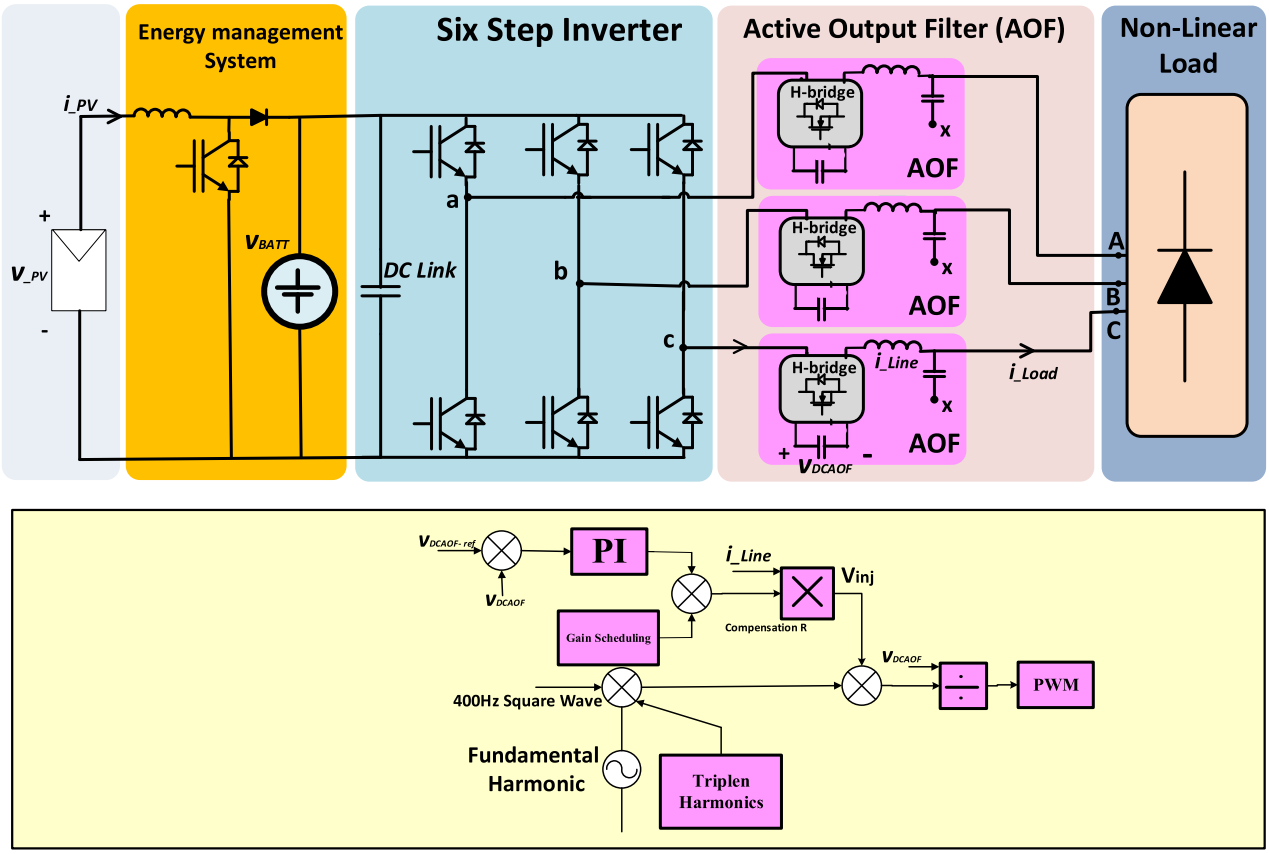

FIGURE 3. Proposed structure of three-phase electric powertrain for solar powered UAV with AOF integration and its closed-loop control strategy.

diagram of the proposed single-phase square wave inverter with one AOF circuit and AC-bus line, while Fig. 2(b) depicts schematic diagram of the three-phase circuit of the proposed system, which consists of three-phase six-step inverter and three individual AOF H-bridge system with AC-bus line. The proposed systems using 400 HZ switching frequency main inverter and AOF systems are employed in UAV for further reduction in the size of the power transmission system under non-linear load conditions with closed loop control.

II. PROPOSED SOLAR POWERED UNMANNED AERIAL VEHICLE

The structure of the proposed three-phase electric powertrain system of the solar powered UAV with its closed-loop control strategy is illustrated in Fig. 3, which indicates that this structure involves two main parts. The first part is the DC side unit producing DC voltage level, which consists of PV array, DC-DC converter, battery, and power management system. The second part is the AC side unit that consists of three-phase six-step inverter with three-individual AOF of H-bridge topology, which generates sinusoidal AC output voltage for the non-linear load represented by the three-phase diode rectifier. The AOF visualized as a power semiconductor active filter block where the standard LC output filter elements are replaced by a series H-bridge topology. The H-bridge is conducted at a high frequency to introduce voltage harmonics in series with each phase to achieve a sinusoidal output voltage for non-linear loads. The non-linearity of loads results from the recent developments of UAV's loads supplied by rectifier circuits.

The proposed power train with AOF has the following advantages:

- Low voltage switching for AOFs semiconductor devices.
- An extreme decrease in the size of the output LC filter due to high switching frequency operation.
- The use of advanced wide-band gap devices in AOF block design enables high performance while simultaneously reducing the component sizes.
- Produces a high-quality sinusoidal voltage waveforms.
- The use of AOF enables the main inverter to be operated in six-steps or at a reduced PWM switching frequency, thus reducing the conduction power loss, and improving the conversion efficiency.
- AOF is dynamic and can be used for retrofitting applications.

In addition, AOF DC-link voltages have the advantage of self-balancing to the third of the DC-link voltage of the main inverter without the need for close-loop control for linear loads. However, the situation is not similar for highly polluted

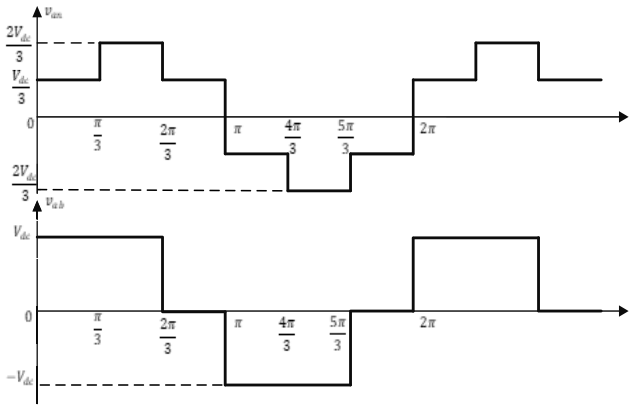

FIGURE 4. Voltage waveforms of six-step inverter.

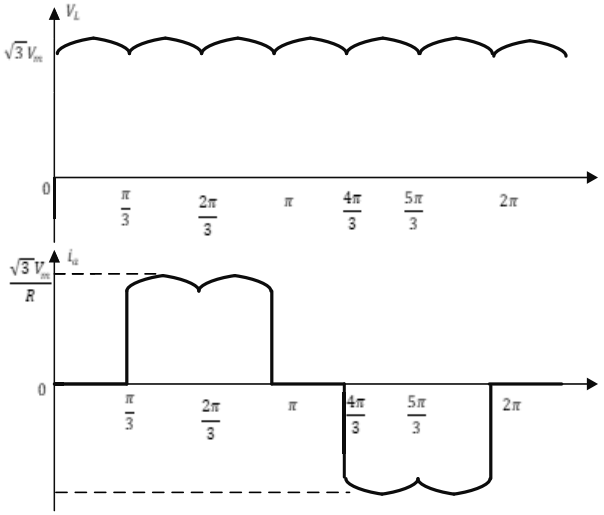

FIGURE 5. Load voltage and line current waveforms of non-linear load.

non-linear loading conditions. Naturally, the non-linear load will advance the current harmonics; These harmonics will be reflected in the AOF DC side. Naturally, the non-linear loads provide current harmonics that will be reflected to AOF DC side, resulting in unbalanced voltage components across the AOF DC link and the line-to-line voltages will be highly distorted. Therefore, AOF topology with open loop control is limited to linear ac loads. In the application of non-linear loads, The AOF-DC link voltage must be controlled to ensure the voltages across the three DC capacitors is balanced at a value of one-third of the DC bus line voltage of the main inverter. Fig. 3 (b) shows the proposed closed-loop control strategy for AOF to produce an active compensation resistance technique, which is used widely in energy conversion control systems [30]. The closed-loop control strategy provides a resistance emulator in series with the H-bridge topology which creates a voltage injection across it to dampen the undesirable harmonics generated from the AOF. This active compensation resistances approaches zero at steady-state operation in the case of linear loads [35]. The DC link

TABLE 1. Simulation constants and circuit parameters.

Parameter		Symbol	Value
DC link voltage (V)		V_{dc}	681
Load voltage (V)		V_o	310
AOf DC-bus capacitor (μF)		C_b	100
Filter inductance (mH)	AOF	L_f	1
	PWM		20
Filter capacitance (μF)	AOF	C_f	40
	PWM		120
Load resistance (Ω)		R_{load}	18.432
AOF switching frequency (kHz)		f_{AOF}	48
Main inverter switching frequency (Hz)		f_{inv}	50
Output frequency (Hz)		f_{load}	400

voltage of the AOF ($V_{dc,AOF}$) is compared to the one-third of the main inverter DC bus-line ($V_{dc,ref}$) as shown in Fig. 3(b) and the error signal is provided to a PI and gain scheduling controllers to create the active compensation resistance. The compensation resistance is multiplied by the line current (i_a) to produce the injected voltage waveform (v_{in}). The injected voltage contains the reflected harmonics from the non-linear load that need to be included in the main AOF control signal. The actual sensed ($V_{dc,AOF}$) voltage is divided by the resulted injected voltage signal obtained previously. Finally, the modeling signal is attained and sent to AOF topology through high switching frequency pulse width modulation technique.

III. ANALYSIS AND MODELING

The main inverter is a six-step switching inverter that is extensively being used to simplify the control circuit and reduce the switching losses. Low odd harmonics of order $n = mp \pm 1$, where, p is the number of pulses ($p = 6$) and m being an integer with the absence of triple-n harmonics ($n = 3, 6, 9, 15, \ldots\ldots$) are generated. The six-step main inverter output line voltage v_{ab} and phase voltage v_{an} waveforms are shown in Fig. 4, the AC output phase voltages consist of discrete values of voltages, which are $\frac{V_s}{3}$, $\frac{2V_s}{3}$, $\frac{-V_s}{3}$, $\frac{-2V_s}{3}$.

The Fourier series expression of the phase voltage v_{an} can be given as:

$$v_{an}(t) = \frac{2V_{dc}}{\pi}\left[\sin(\omega t) + \frac{1}{5}\sin(5\omega t) + \frac{1}{7}\sin(5\omega t) + \ldots\right] \quad (1)$$

$$v_{an}(t) = \sum_{k=1,5,7,11\ldots}^{\infty} \frac{2V_{dc}}{\pi k}\sin(k\omega t) \quad (2)$$

To produce a pure sinusoidal output voltage waveform, the injected voltage of the AOF should be equal in magnitude and opposite in sign to the harmonic contents of the six-step inverter given by Eq. (2). Therefore, the AOF should be controlled to inject the harmonics of orders 5th, 7th, ...and

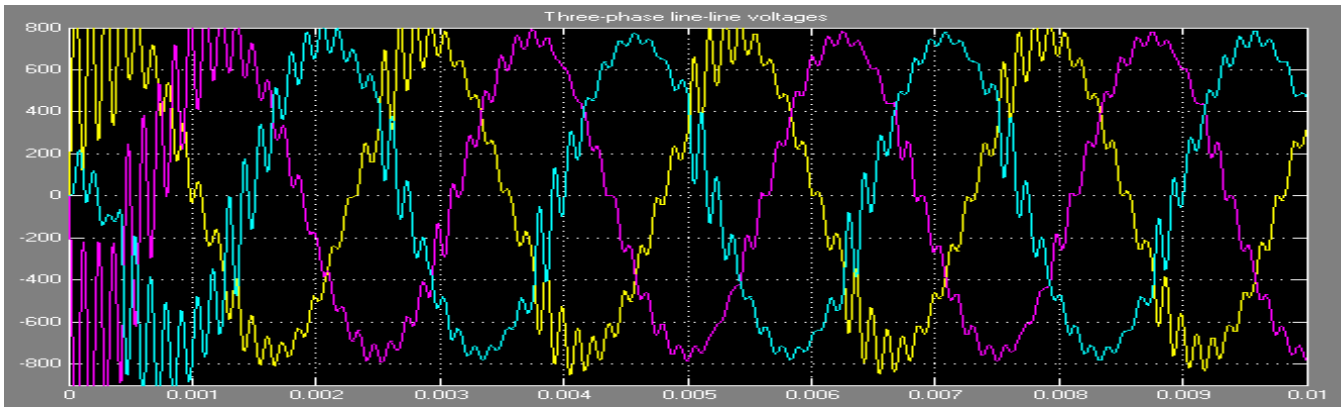

FIGURE 6. Three-phase line voltages with open-loop control.

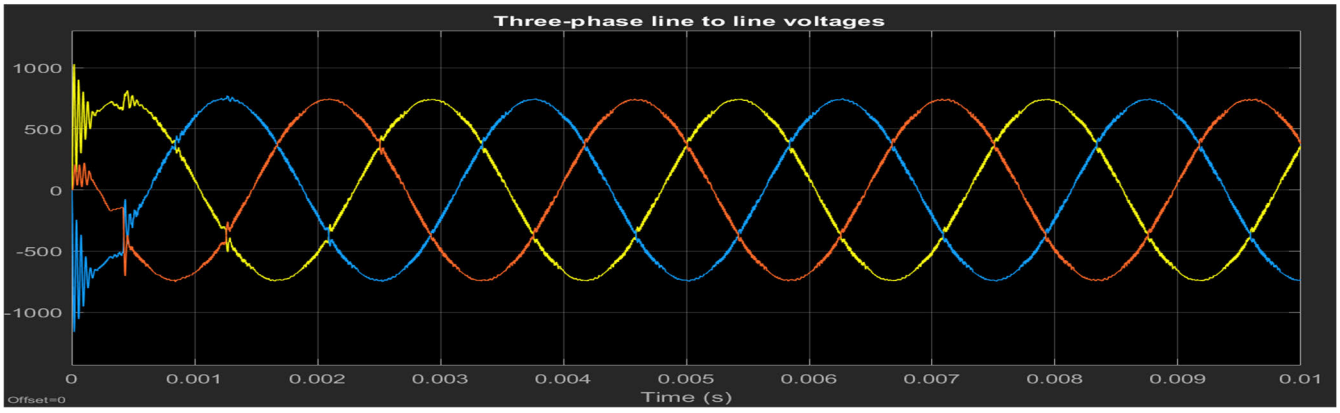

FIGURE 7. Three-phase line voltages with closed loop control.

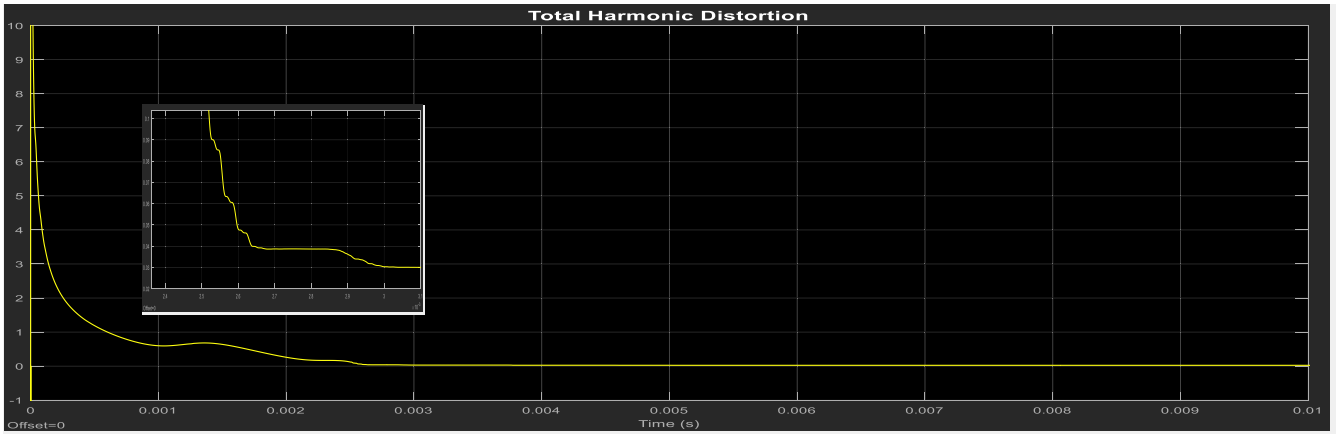

FIGURE 8. Total harmonic distortion.

nth, with the magnitude of $\frac{2V_{dc}}{\pi k}$, as:

$$v_{AOF}(t) = -\sum_{k=5,7,11...}^{\infty} \frac{2V_{dc}}{\pi k} \sin(k\omega t) \tag{3}$$

The total output voltage across the load terminal is the summation of the inverter output voltage and the AOF produced voltage, and it will be a pure sinusoidal waveform as:

$$v_O(t) = v_{an}(t) + v_{AOF}(t) \tag{4}$$

$$v_O(t) = \frac{2V_{dc}}{\pi} V_{dc} \sin(\omega t) \tag{5}$$

Neglecting the ripple at the DC side of the AOF, the switching function $S_{AOF}(t)$ of the AOF can be obtained by dividing

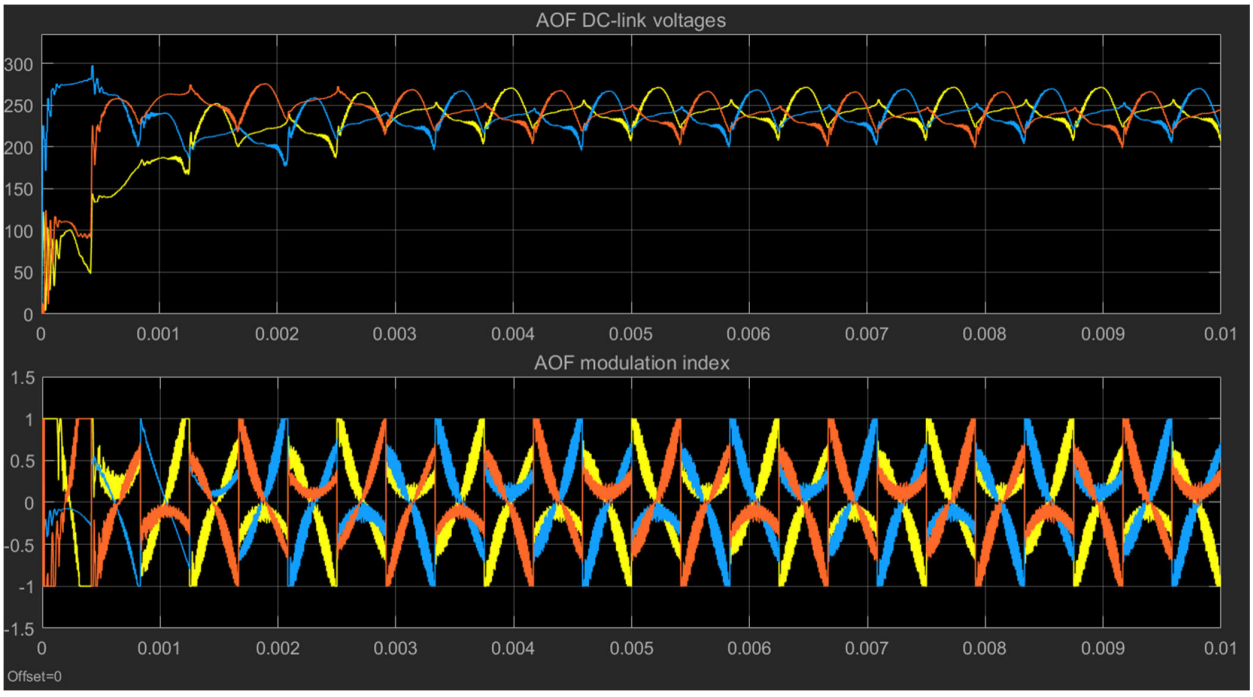

FIGURE 9. The DC-bus voltages (upper trace) and modulation index (lower trace) of AOF.

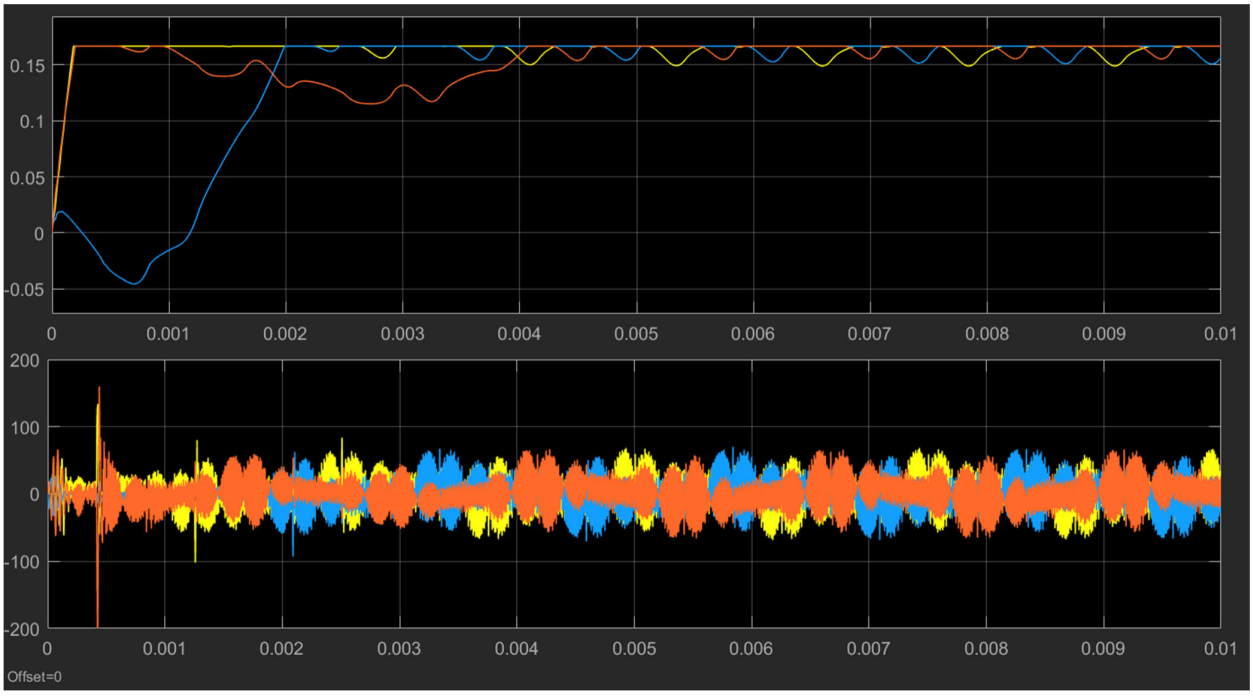

FIGURE 10. Active compensation resistance (upper trance) and AOF injected voltage (lower trace).

the AOF injected voltage with the AOF voltage at the DC side as:

$$S_{AOF}(t) = \frac{v_{AOF}}{V_{dc,AOF}} = -\sum_{k=5,7,11\ldots}^{\infty} \frac{2V_{dc}}{\pi k V_{dc,AOF}} \sin(k\omega t) \quad (6)$$

The AOF dc side voltage $V_{dc,AOF}$ is controlled at the third of the six-step inverter supply voltage ($\frac{V_{dc}}{3}$), and assuming ripple free AOF DC link voltage, the switching function $S_{AOF}(t)$ of the AOF can be simplified as:

$$S_{AOF}(t) = -\sum_{k=5,7,11\ldots}^{\infty} \frac{6}{\pi k} \sin(k\omega t) \quad (7)$$

The non-linear load is represented by a three-phase bridge rectifier, which is used in medium to high-power application.

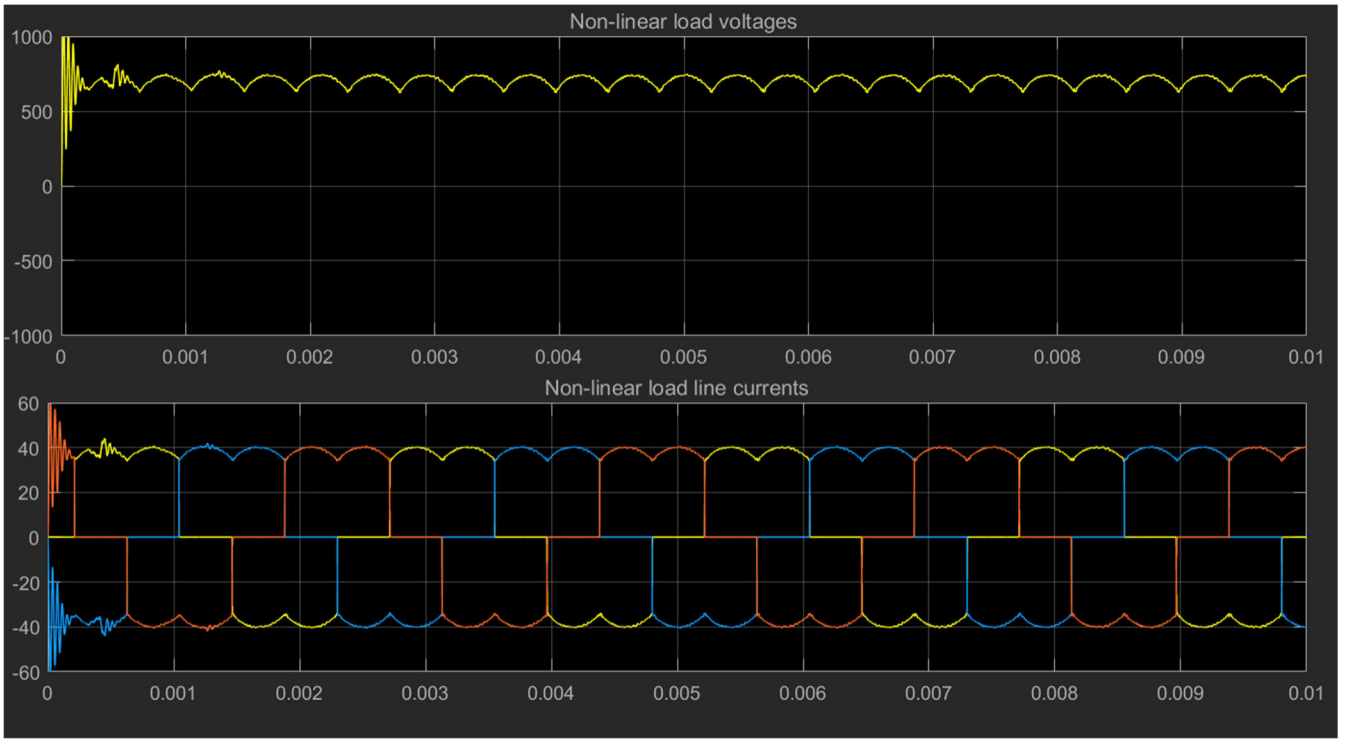

FIGURE 11. Voltage and current waveforms of three phase non-linear load.

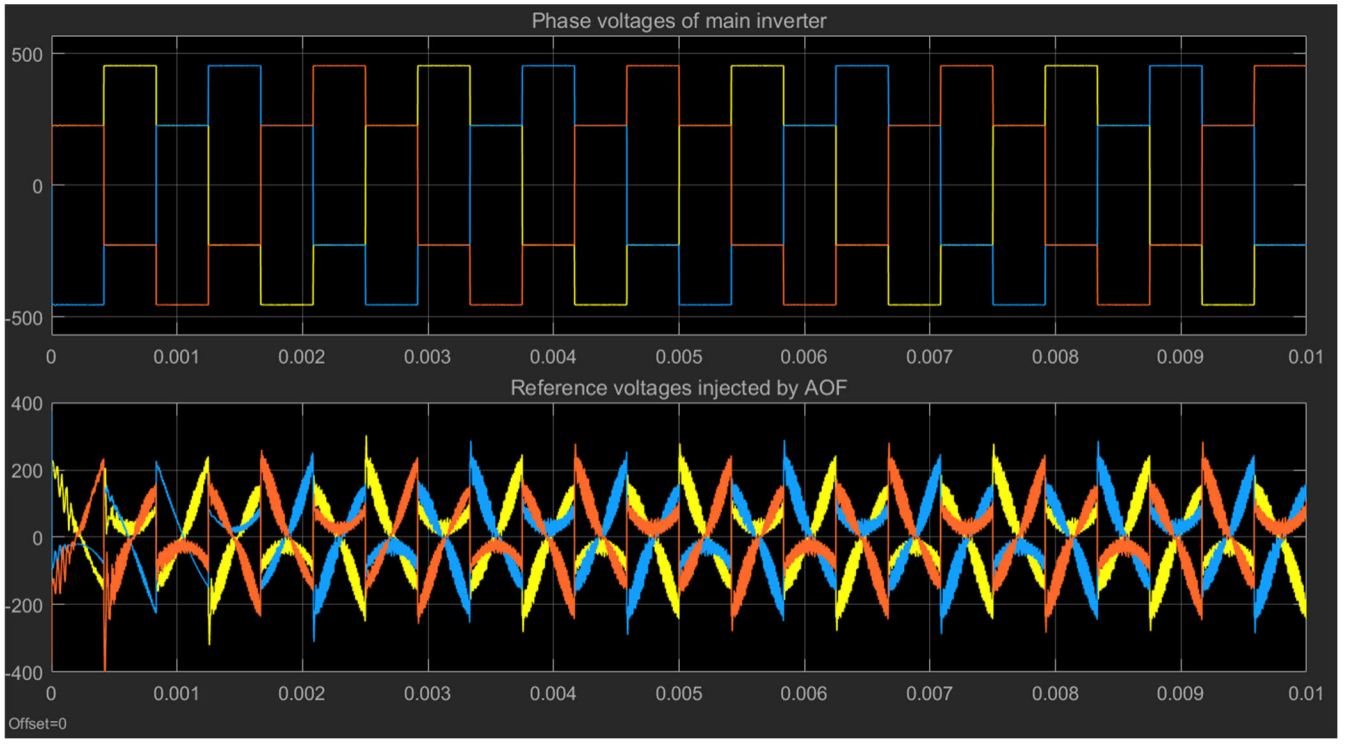

FIGURE 12. Main inverter voltages and AOF injected voltages.

It produces a six-pulse ripples on the load voltage waveform having the highest value of the instantaneous line voltage of the supply voltage. The waveforms of the load voltage and ac side line current are shown in Figure 5, where V_m is the maximum phase voltage which is equal to the maximum value of the fundamental component of the six-step inverter $\frac{2V_{dc}}{\pi}$.

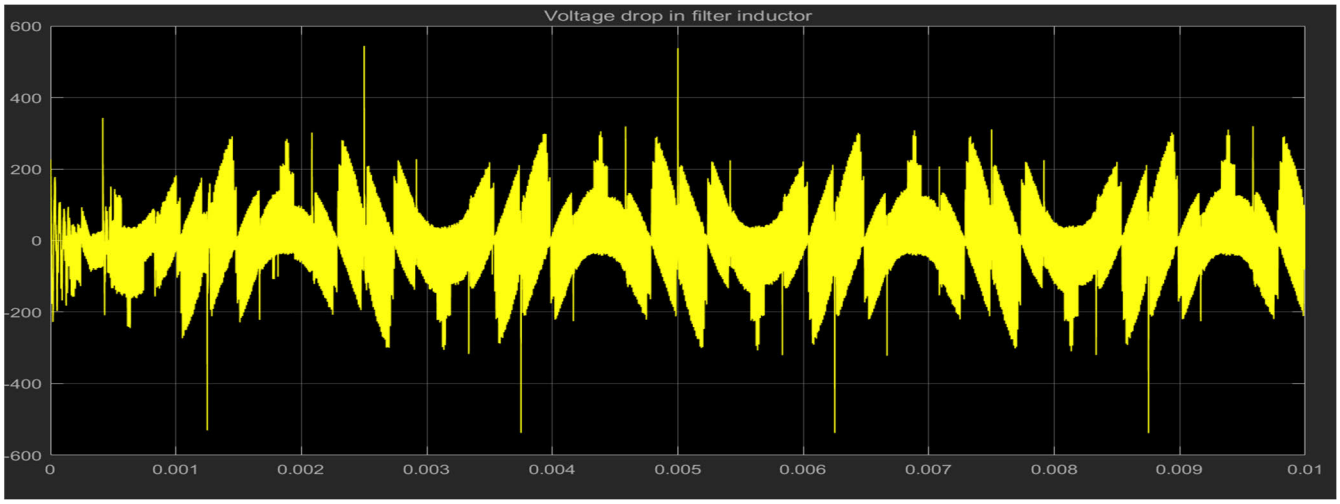

FIGURE 13. Voltage drop in the filter inductor.

TABLE 2. Semiconductor losses of AOF and PWM inverter.

R_{load}	Conduction losses		Switching losses		Total losses		Power loss reduction
	AOF	PWM	AOF	PWM	AOF	PWM	
18.432	1413	424	3924	7356	5337	7780	31%

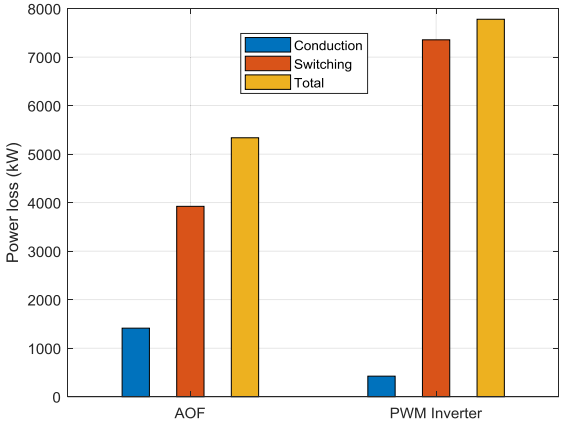

FIGURE 14. Comparison of semiconductor power losses at rated power.

The line current shown in Fig. 5 can be described by the Fourier series as

$$i_a(t) = = \frac{2\sqrt{3}V_{dc}}{\pi R}\left[\sin(\omega t) - \frac{1}{5}\sin(5\omega t) - \frac{1}{7}\sin(7\omega t) + \frac{1}{11}\sin(11\omega t) + \frac{1}{13}\sin(13\omega t)\ldots\ldots\right] \quad (8)$$

$$i_a(t) = \sum_{k=1,5,7,11\ldots}^{\infty} \pm\frac{2\sqrt{3}V_{dc}}{\pi kR}\sin(k\omega t) \quad (9)$$

The plus or minus sign, symbol "±," mentions that some terms of the line current harmonics may be added or subtracted depending on its order and the rule can be inferred from the first few terms. The DC link current of the AOF can

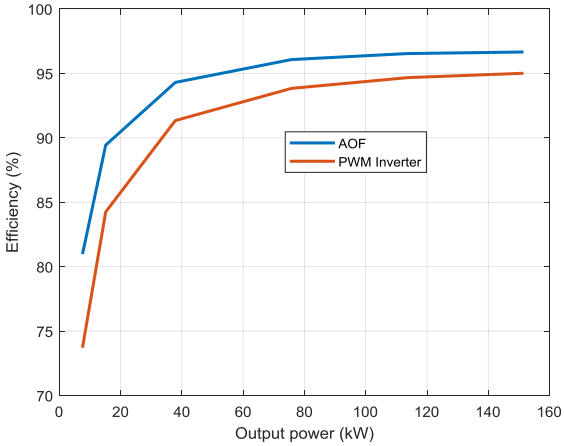

FIGURE 15. Comparison of power conversion efficiency of AOF system and traditional PWM inverter at different load powers.

be achieved by multiplying the switching function $S_{AOF}(t)$ that controls the AOF and the ac current of $i_a(t)$ as:

$$i_{dc,AOF}(t) = S_{AOF}(t).i_a(t) \quad (10)$$

$$= -\sum_{k=5,7,11\ldots}^{\infty}\frac{6}{\pi k}\sin(k\omega t) \times \sum_{n=1,5,7,11\ldots}^{\infty}\pm\frac{2\sqrt{3}V_{dc}}{\pi nR}\sin(n\omega t) \quad (11)$$

$$= -\frac{12\sqrt{3}V_{dc}}{\pi^2 R}\sum_{k=5,7,11\ldots}^{\infty} \times \sum_{n=1,5,7,11\ldots}^{\infty}\pm\frac{1}{nk}\sin(k\omega t) \quad (12)$$

IV. SIMULATION RESULTS

To investigate the principle of operation and to verify the effectiveness of the proposed powertrain system, the total system shown in Fig. 3 is simulated in MATLAB Simulink under

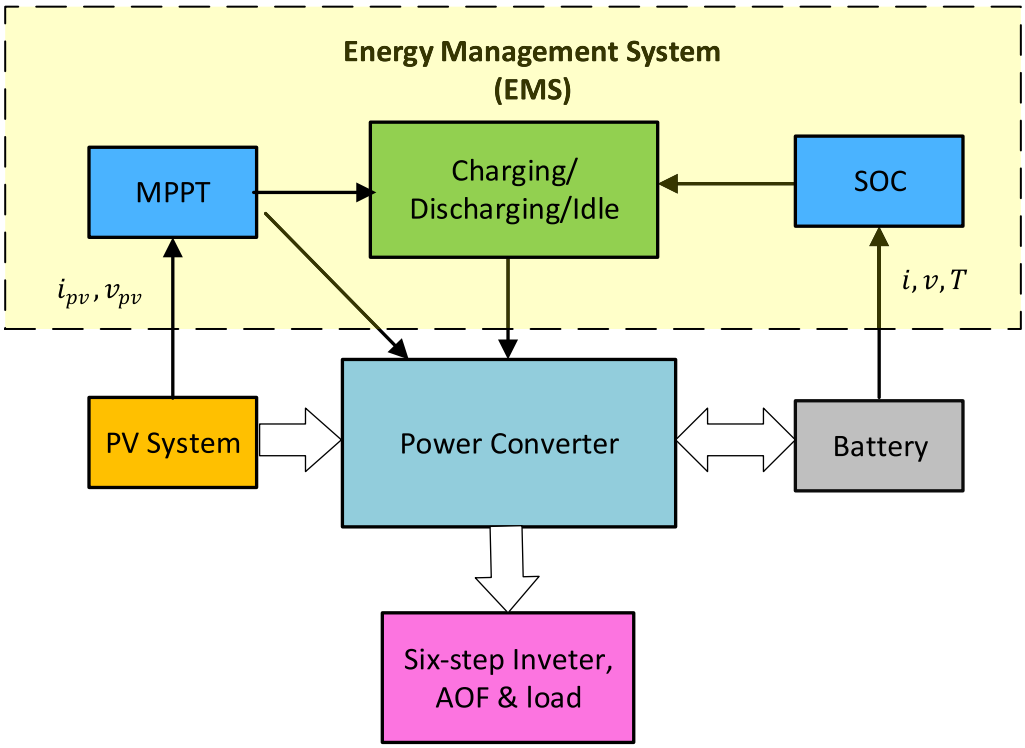

FIGURE 16. Power management function block diagram.

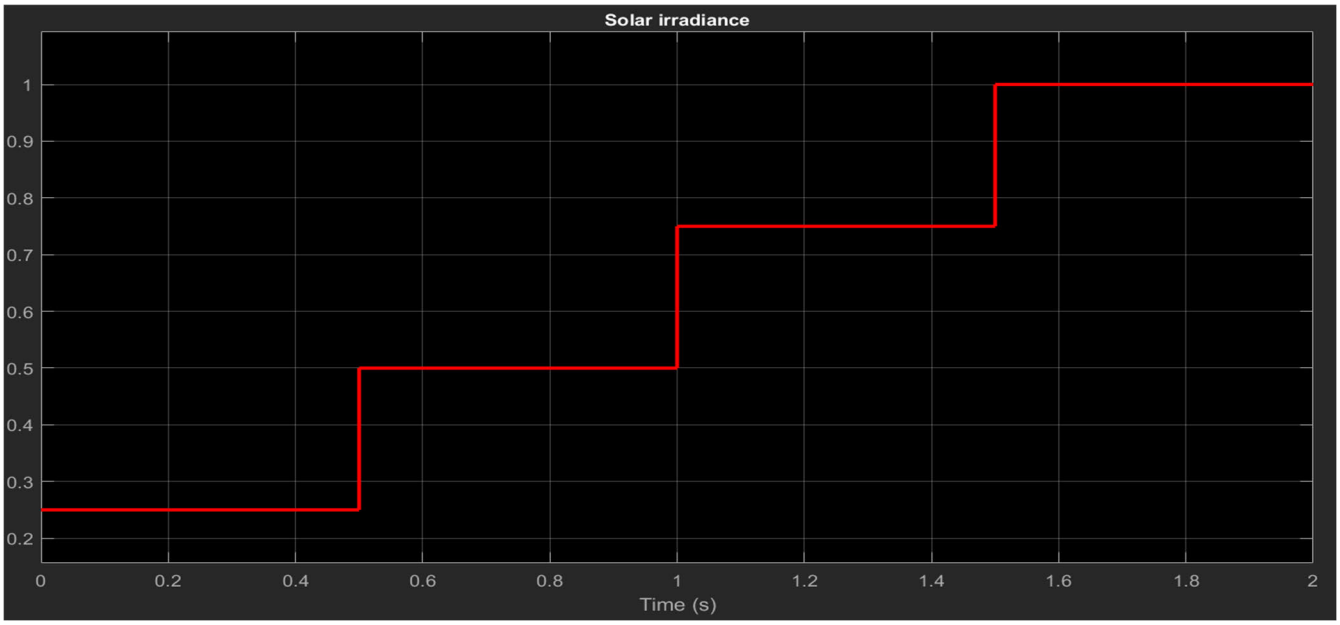

FIGURE 17. Tested insolation conditions for UAV PV power system.

closed-loop control and a load of three-phase diode bridge rectifier. The solar PV and Energy management system has been represented by an ideal dc voltage source. The simulation is carried out for the simulation constants and circuit parameters listed in Table 1.

The three-phase line to line voltages at the terminal of the non-linear load of three-phase diode rectifier at open-load operation conditions are shown in Fig. 6. It can be noticed that voltage waveforms are highly distorted due to the DC-link voltage unbalance of the AOF. The waveforms of the same line voltages at closed-loop control operation are shown in Fig. 7. The line voltages have high-quality sinusoidal waveforms with total harmonic distortion less than 3% as shown in Fig. 8. Fig. 9 depicts the three DC-bus line voltages

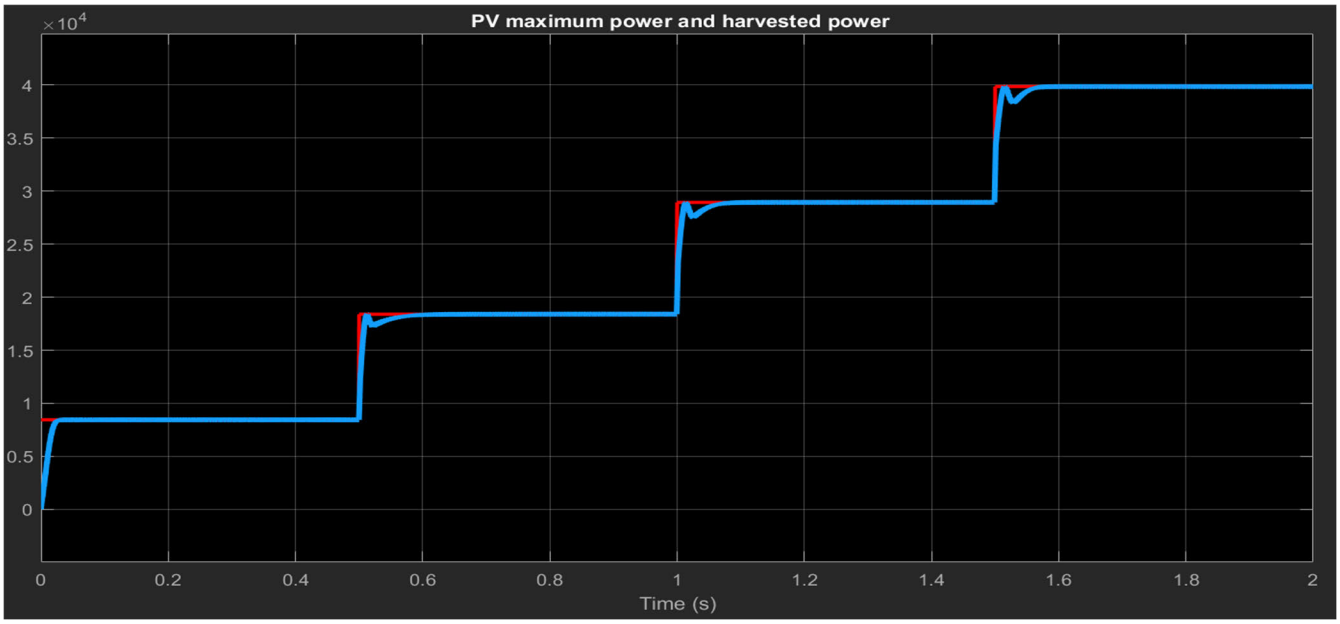

FIGURE 18. PV harvested power.

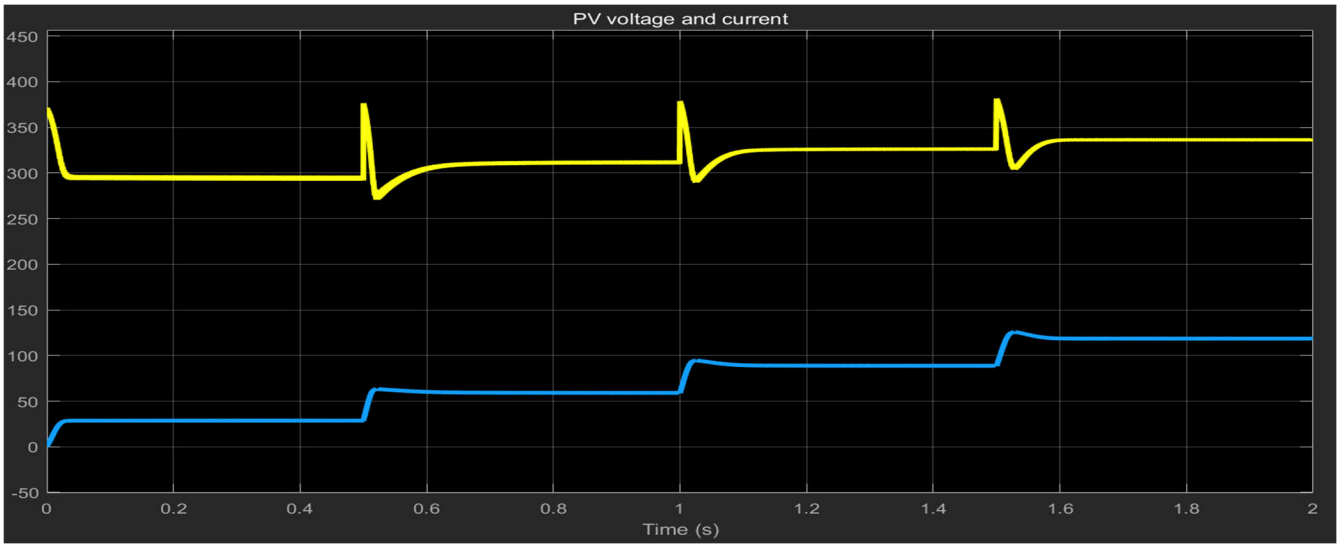

FIGURE 19. PV voltage (upper trace) and current (low trace).

($V_{dc,AOF}$) of the AOF filter and the modulation index. It can be observed that the capacitors voltages are balanced and settled to one-third of the DC-bus line voltage at steady-state conditions. The DC-bus voltages of the AOF and its modulation index are illustrated in Fig. 10, which indicates that the dc-link voltage of the AOF settles at the third of the main inverter supply voltage ($\frac{V_{dc}}{3}$) and the AOF dc-link current does not include a dc component as it is clear from equation (13). Fig. 11 shows the active compensation resistance and the injected phase voltage (V_{inj}) across this damping resistance. The load side DC voltage and the corresponding three-phase ac line currents at the input of the rectifier (non-linear load) for a resistive load are depicted in Fig. 12. It can be confirmed that the line currents are consistent with the well-known three-phase diode bridge rectifier under sinusoidal supply voltage as illustrated in Fig. 5 The dc load voltage waveform is as expected with a ripple frequency of 2400Hz i.e. six times that of the 400Hz of the main six-step inverter frequency. The three-phase main inverter voltages and the three phase injected voltages by AOF are shown in Fig. 12. The voltage drop across the filter inductor with zero dc component is shown in Fig. 13.

A. POWER LOSS ANALYSIS

This section emphasizes on power loss analysis and conversion efficiency comparison with traditional PWM inverter. Power semiconductor devices are highly non-ideal which leads to significant power loss. The power semiconductor

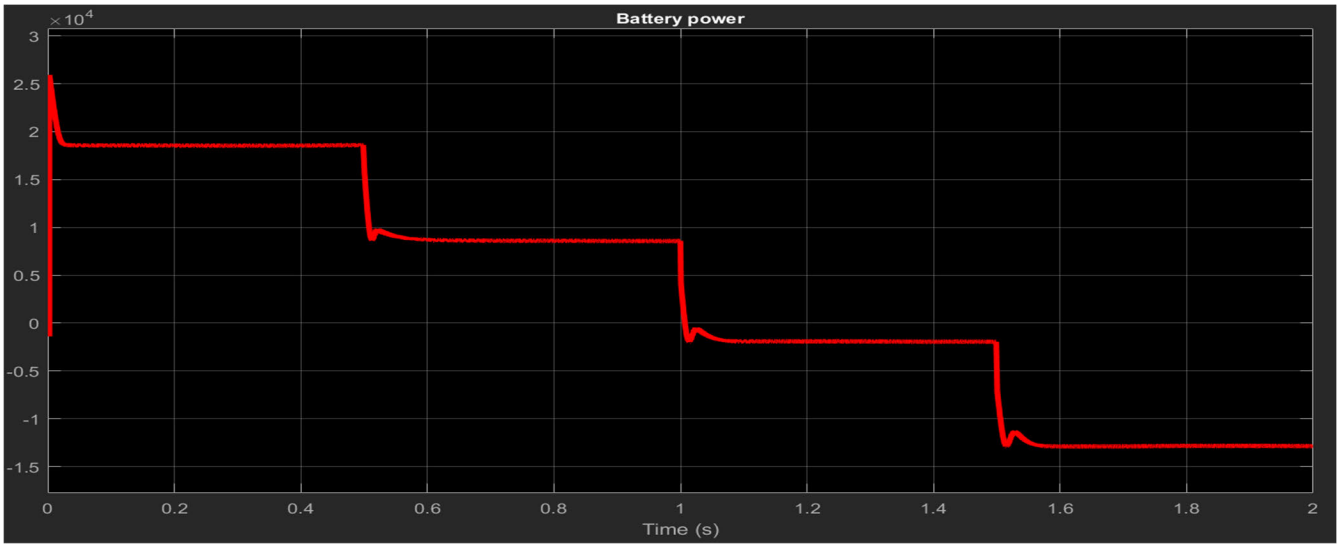

FIGURE 20. Battery power.

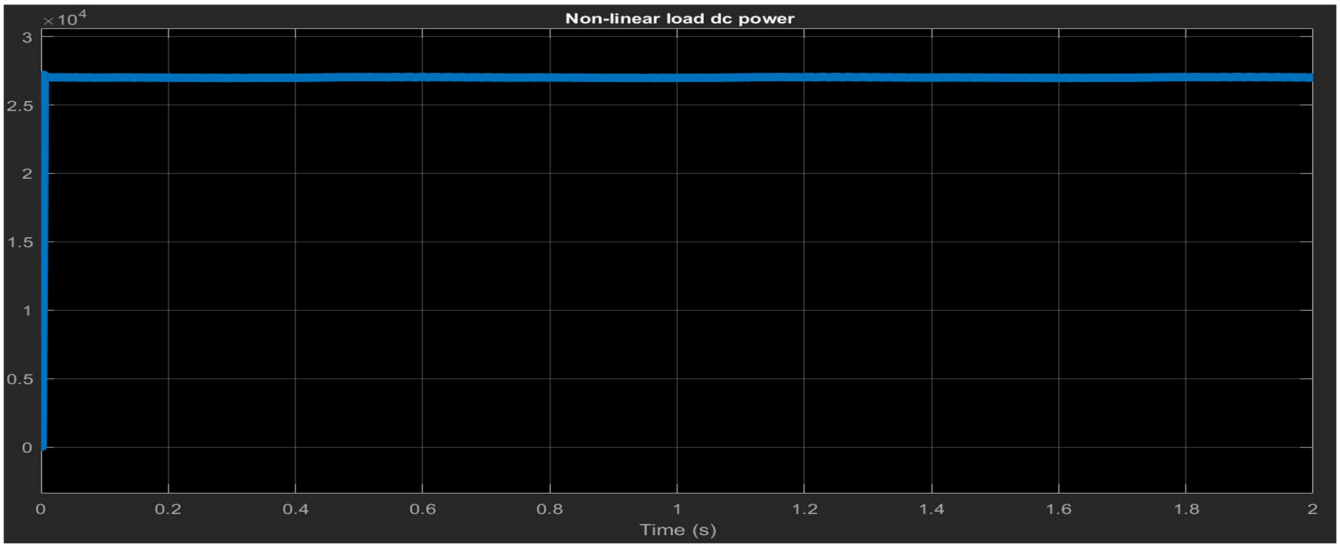

FIGURE 21. Non-linear load output dc power.

losses including conduction losses and switching losses are considered and the LC filter components losses are not considered in this paper. The switching losses can be calculated by estimating the power loss per switching period and then summing them. Various methods have been established to estimate the power losses in the semiconductor devices. Loss estimation can be done by analyzing the electrical behavior of the currents and voltages waveforms of the circuit or using numerical simulation using special simulation programs that incorporated loss computation tools. In addition, manufacturer datasheets contain information about the power loss calculation that can be used efficiently to calculate the power losses in the semiconductor devices. In this paper, the power loss calculation is carried out using the thermal analysis method integrated with PSIM Software. Fig. 14 and Table 2 show the comparison of semiconductor conduction, switching and total power losses of the proposed powertrain based AOF system and the traditional PWM inverter at rated power. From Fig. 14, it is clear to note that the main contribution of power losses is due to switching loss. The total semiconductor power loss of the AOF based system is reduced by the ratio of 31% compared to the conventional PWM inverter. Fig. 15 shows the comparison of power conversion efficiency at different loading conditions. It is clear to notice that the power conversion efficiency of the AOF system is improved significantly at all operating power range.

B. SOLAR POWERED UNMANNED AERIAL VEHICLE (UAV)

As a further step toward the complete UAV power system includes solar PV and Energy management system, the solar powered UAV system shown in Fig. 3 has been investigated. The PV power, which is dependent mainly on the solar radiation, is changeable and unsteady. Therefore, a storage system of rechargeable batteries is indispensable to provide

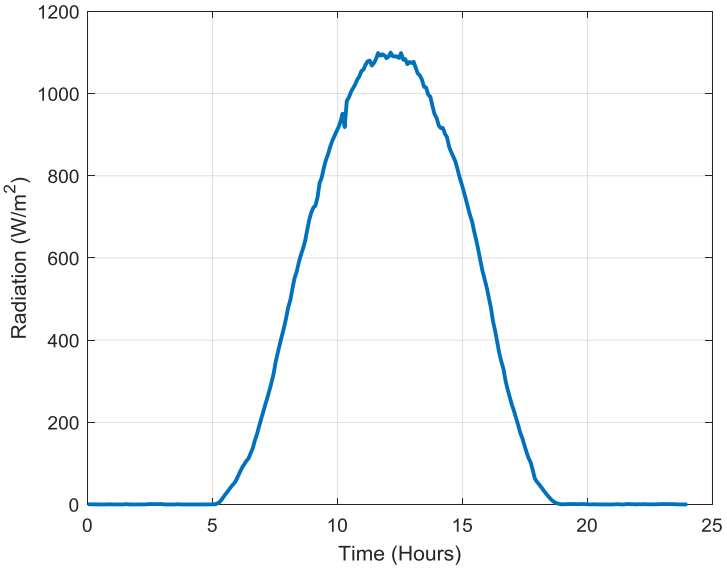

FIGURE 22. Solar radiation during 1st August.

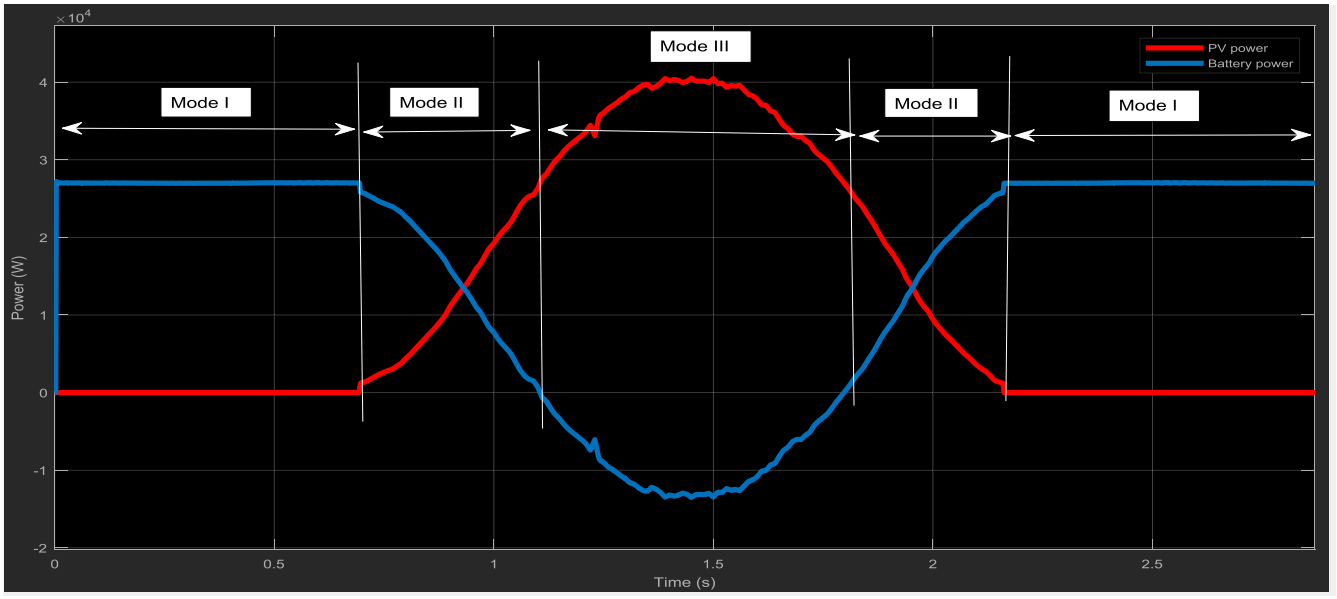

FIGURE 23. PV harvested power during different operating modes.

the required power for UAV when PV power is unavailable during night hours or during cloudy days. The batteries store the PV power during sunny day hours, and then discharge to power the aircraft during night hours or the daytime with insufficient solar radiation. The storage system consists of several batteries connected in series or parallel based on the load demands. The aircraft power comes mainly from the PV system as primary source of energy and secondary from the battery storage system. The optimal size of the batteries and the PV array are hard to be specified because the PV power depends on the solar radiation which varies from season to season and from region to region. In this paper, a reasonable size of the PV array is selected to produce 40 kW at a standard solar insolation of 1000W/m^2 to supply a power of 27kW to the UAV DC-bus line and 13kW access power is utilized to charge the battery through the energy management system (EMS). The EMS can accomplish the purpose of maximum power point tracking (MPPT) and manages the flow of power PV system, storage battery and load. The schematic block diagram of the EMS and the DC side of the proposed system is shown in Fig. 16. Based on the flow of power through the PV system, storage battery and load, the operation modes can be divided into four modes of operation.

1) MODE I

During night hours or during days with insufficient solar radiation or bad weather conditions, the total power is provided by the storage system and the PV system does not provide any power.

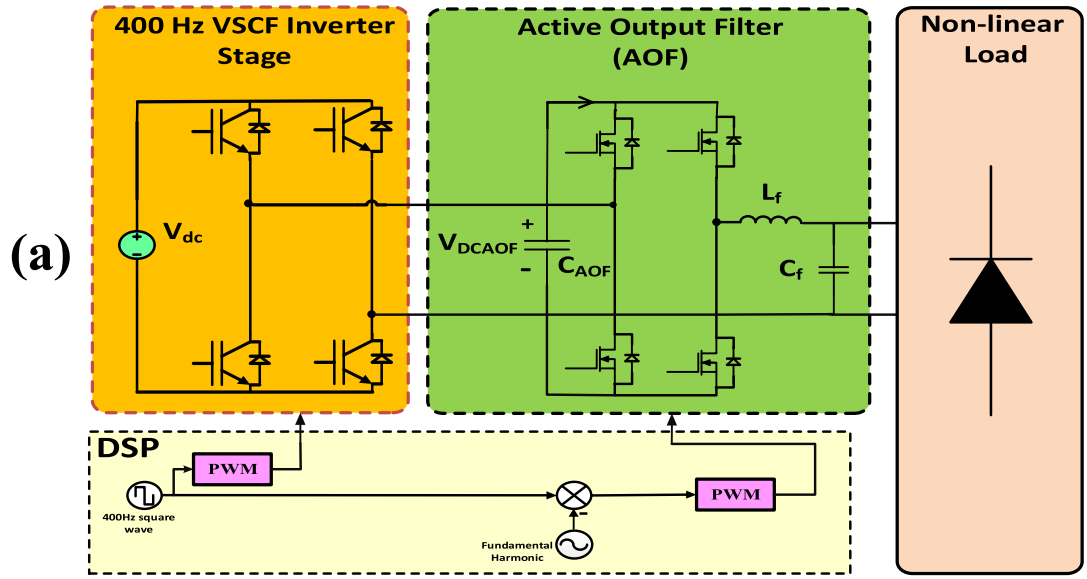

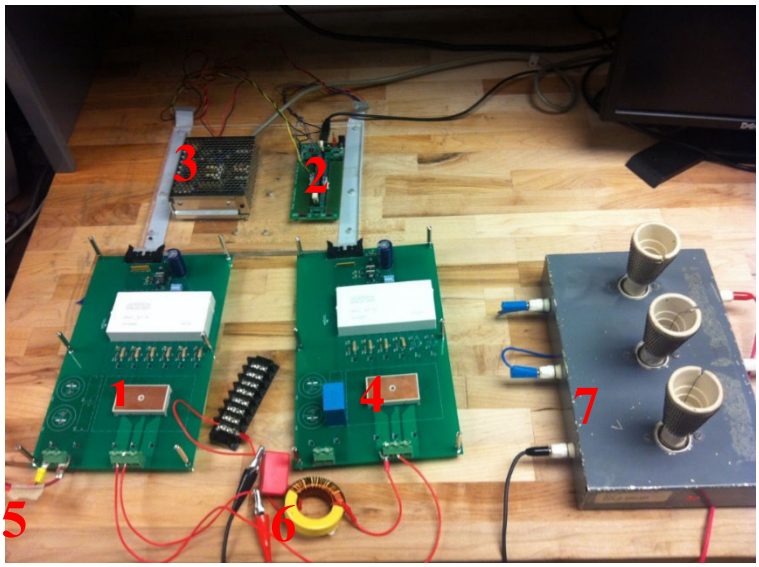

1	Main Inverter H Bridge
2	TIF28335 DSP
3	15v DC Supply
4	AOF H-Bridge
5	Input DC
6	L-C Filter
7	Resistive load
8	Diode bridge rectifier

FIGURE 24. Setup of experimental system: (a) shows schematic diagram of the implemented setup. (b) depicts reduced size experimental prototype.

2) MODE II

This mode is defined when the solar radiation is available, but it is not enough, during morning or evening periods or even during cloudy weather. PV system can provide power, but it is also not enough for powering the load. During this mode, the load power is shared by both PV system and storage system. The PV system is the main energy system and the storage supplements the deficit power between the load and the PV system.

3) MODE III

During sunny days with sufficient solar radiation, the PV system can generate enough power to the load and the excessive PV power is spent in charging the battery system if the batteries are not fully charged., This is decided by the battery state of charge (SOC).

4) MODE IV

When the aircraft is not working or during the fully charged case of battery system, the EMS stops the PV power harvesting and Battery charging to keep battery system safe. The battery charging mode will automatically turn off once the battery is fully charged, according to the battery charging specifications.

The full system has been simulated at different insolation conditions and the results are verified in Figs. 17 to 21. Fig. 17 shows the step change of insolation that changes from 250, to 1000W/m^2 in a step of 250 W/m^2. The perturbation and observation (P&O) maximum power point tracking is used in this paper for its simple structure and ease of implementation [36]. Fig. 18 illustrates the corresponding maximum PV power and the PV harvested power. It can be confirmed that the harvested power tracks the maximum

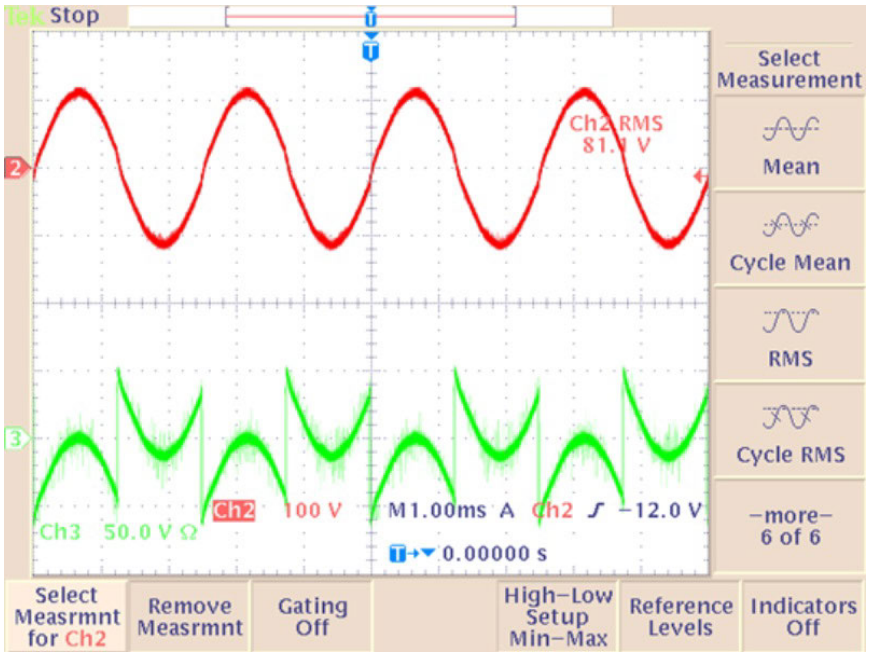

FIGURE 25. Experimental waveforms of sinusoidal output voltage (upper trace) and AOF injected voltage (lower trace) for linear load.

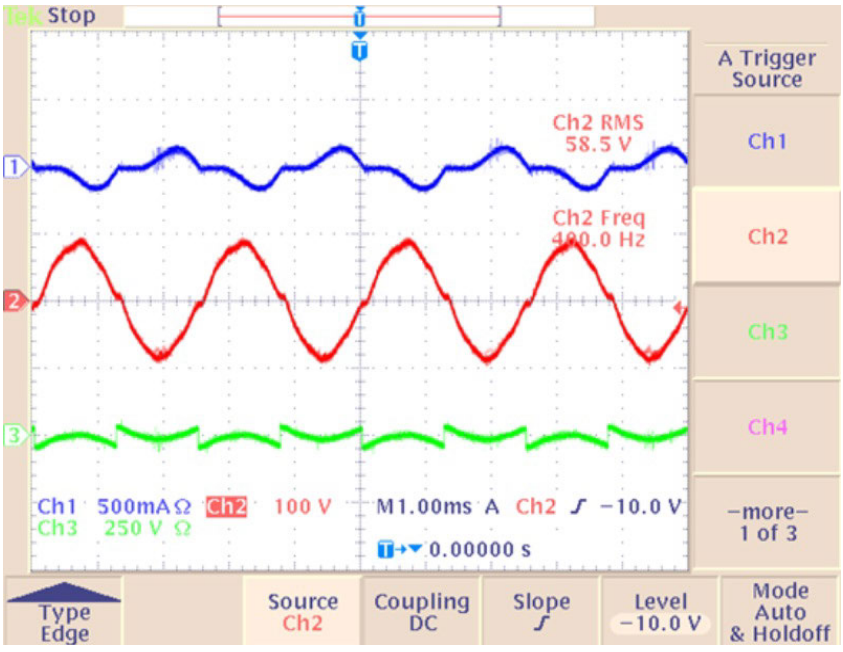

FIGURE 26. Experimental waveforms of (a) line current voltage (upper trace), (b) output voltage (middle trace) and (c) AOF injected voltage (lower trace) for non-linear load.

power very well. A conventional incremental conductance maximum power point tracking technique is used in this work, while the relevant voltage and current of the PV system are shown in Fig. 19. Fig. 20 shows the processed power of the battery through the energy management system such that the battery supplies the load during low insolation conditions, while stores access energy at high solar insolation conditions. Fig. 21 shows the non-linear load DC output power.

In addition, the operation of the solar powered UAV has been studied during a sunny summer day to show the different operation modes based on the power flows among PV system, batteries and load under different radiations conditions. Fig. 22 shows the measured solar radiations measured every 5 minutes during the 1st of August. Fig. 23 shows the PV harvested power and the battery power, where the battery power is positive during discharging when the power is realized from the battery to the load. The battery power is negative when

battery is charging, and the power is stored in the battery. Also, Fig. 23 shows the operating modes during 24 hours of a sunny day. During evening or early morning when the solar radiation is less than 50 W/m2, no power is generated by the PV system and all the load power is supplied by the batteries and the system operates in Mode I and the battery is in discharging mode. Mode II starts when the solar radiation reaches 50 kW/m^2 or more and the load power is supplied by both PV system and battery. In this mode PV system generates power but it is not enough to power the load and the battery also is in discharging mode. In mode III, the PV harvested power is greater than the load power and part of this power supplies the load and the other part is derived in charging the battery.

V. EXPERIMENTAL RESULTS

To verify the principle of operation and the validation, the proposed closed-loop powertrain system for solar powered UAV is tested experimentally on a reduced downsized 1.2kVA power rating single-phase square wave prototype. Fig. 24 shows the experimental setup proposed to test the powertrain system of the solar powered UAV shown in Fig. 3. The TIF28335 digital signal processor (DSP) manufacture by Texas Instrument is used and two GPIO registers have been used to drive the semiconductor switches of the main 400Hz main inverter and PWM driving signals have been used for the AOF H-bridge switches. The 400Hz main inverter and AOF H-bridge switches have been implemented using ''SKHI-61R SEMEKRON 10KW'' inverter modules and SEMEKRON ''SKHI-61R'' gate drives powered by 15V DC supply are used for driving and isolation. A ''B&K Precision XLN10014'' DC power supply that is capable to supply up to 100V, 14A load is employed. Fig. 24 shows the experimental waveforms of sinusoidal output voltage and AOF injected voltage for linear load and Fig. 26 shows the experimental waveforms of line current, output voltage and AOF injected voltage in the case of non-linear load. It is clear to notice that the output voltage has a high-quality sinusoidal waveform with a total harmonic distortion less than 5% in the case of resistive load (Fig. 25). For the case of non-linear load, the line current is operated in discontinuous conduction mode keeping acceptable load voltage quality and the load voltage quality is slightly degraded due to low order harmonics generated by the line current of the non-linear load.

VI. CONCLUSION

A new electric power generation system for solar powered unmanned aerial vehicle (UAV) using active output filter has been proposed and investigated in this paper. The proposed power generation system is a potential progress of both the Solong and Zyphyr UAV models using the AC-bus line instead of the DC-bus line to power the propellers. It includes solar PV system, lithium-sulfur based power management system, inverter, AC bus-line. Balanced DC-link voltages of AOF have been accomplished using closed loop control of active resistance compensation, which produces an injected voltage across it to diminish unwanted harmonics created from the non-linear load. The obtained simulation and experimental results and the voltage and current waveforms demonstrated the viability and the correctness of the proposed power generation system. The proposed active resistance compensation ensures a high-quality sinusoidal line voltage with total harmonic distortion less than 3%. Moreover, power loss analysis and conversion efficiency of the proposed system are performed and compared with that of the conventional three-phase PWM inverter. The obtained results proved that the power loss is reduced by 31%. More investigation of the proposed AOF for large-scale PV plants application with Battery energy management system integration using different wide band gab devices to optimize the system efficiency are required with applying different PWM techniques to utilize the passive elements sizing design which are the subject of future work.

REFERENCES

[1] U. Burup, P. N. Enjeti, and F. Blaabjerg, ''A new space-vector-based control method for UPS systems powering nonlinear and unbalanced loads,'' *IEEE Trans. Ind. Appl.*, vol. 37, no. 6, pp. 1864–1870, Nov./Dec. 2001, doi: 10.1109/28.968202.

[2] D. Zhang, J. He, and D. Pan, ''A megawatt-scale medium-voltage high-efficiency high power density 'SiC+Si' hybrid three-level ANPC inverter for aircraft hybrid-electric propulsion systems,'' *IEEE Trans. Ind. Appl.*, vol. 55, no. 6, pp. 5971–5980, Nov. 2019, doi: 10.1109/TIA.2019.2933513.

[3] M. N. Boukoberine, Z. Zhou, and M. Benbouzid, ''A critical review on unmanned aerial vehicles power supply and energy management: Solutions, strategies, and prospects,'' *Appl. Energy*, vol. 255, no. 1, pp. 1–22, Dec. 2019, doi: 10.1016/j.apenergy.2019.113823.

[4] X. Zhao, J. M. Guerrero, and X. Wu, ''Review of aircraft electric power systems and architectures,'' in *Proc. IEEE Int. Energy Conf. (ENERGYCON)*, Cavtat, Croatia, May 2014, pp. 949–953, doi: 10.1109/ENERGYCON.2014.6850540.

[5] O. D. Dantsker, S. Imtiaz, and M. Caccamo, ''Electric propulsion system optimization for long-endurance and solar-powered unmanned aircraft,'' in *Proc. AIAA Propuls. Energy Forum (EATS)*, Indianapolis, IN, USA, Aug. 2019, pp. 1–24, doi: 10.2514/6.2019-4486.

[6] E. E. Evale, S. Thomas, M. S. Lawal, G. E. Abbe, and E. C. Ashigwuike, ''A novel design technique for electrical power system of ABT-18 unmanned aerial vehicle,'' in *Proc. IEEE 3rd Int. Conf. Electro-Technol. Nat. Develop. (NIGERCON)*, Owerri, Nigeria, Nov. 2017, pp. 1120–1124, doi: 10.1109/NIGERCON.2017.8281975.

[7] B. Luckett, J. He, and R. W. Dyson, ''High-efficiency turboelectric propulsion drive based on medium-voltage SiC indirect matrix converter,'' in *Proc. AIAA Propuls. Energy Forum (EATS)*, New Orleans, LA, USA, Aug. 2020, pp. 1–7.

[8] A. Griffo, R. Wrobel, P. H. Mellor, and J. M. Yon, ''Design and characterization of a three-phase brushless exciter for aircraft starter/generator,'' *IEEE Trans. Ind. Appl.*, vol. 49, no. 5, pp. 2106–2115, Sep. 2013, doi: 10.1109/TIA.2013.2269036.

[9] L. Zhu, D. Jiang, R. Qu, L. M. Tolbert, and Q. Li, ''Design of power hardware-in-the-loop simulations for integrated starter–generator systems,'' *IEEE Trans. Transport. Electrific.*, vol. 5, no. 1, pp. 80–92, Mar. 2019, doi: 10.1109/TTE.2018.2881052.

[10] Z. Hao, X. Wang, and X. Cao, ''Harmonic control for variable-frequency aviation power system based on three-level NPC converter,'' *IEEE Access*, vol. 8, pp. 132775–132785, Jun. 2020, doi: 10.1109/ACCESS.2020.3005192.

[11] Z. Zhang, Y. Liu, and J. Li, ''A HESM-based variable frequency AC starter-generator system for aircraft applications,'' *IEEE Trans. Energy Convers.*, vol. 33, no. 4, pp. 1998–2006, Dec. 2018, doi: 10.1109/TEC.2018.2867906.

[12] A. Eid, H. El-Kishky, M. Abdel-Salam, and M. T. El-Mohandes, ''On power quality of variable-speed constant-frequency aircraft electric power systems,'' *IEEE Trans. Power Del.*, vol. 25, no. 1, pp. 55–65, Jan. 2010, doi: 10.1109/TPWRD.2009.2031672.

[13] Z. Zhang, J. Li, Y. Liu, Y. Xu, and Y. Yan, "Overview and development of variable frequency AC generators for more electric aircraft generation system," *Chin. J. Electr. Eng.*, vol. 3, no. 2, pp. 32–40, Sep. 2017, doi: 10.23919/CJEE.2017.8048410.

[14] A. S. Mohamad, "Modeling of a steady-state VSCF aircraft electrical generator based on a matrix converter with high number of input phases," in *Proc. IEEE Student Conf. Res. Develop. (SCOReD)*, Kuala Lumpur, Malaysia, Dec. 2015, pp. 500–505, doi: 10.1109/SCORED.2015.7449387.

[15] V. Biagini, P. Zanchetta, M. Odavic, M. Sumner, and M. Degano, "Control and modulation of a multilevel active filtering solution for variable-speed constant-frequency more-electric aircraft grids," *IEEE Trans. Ind. Informat.*, vol. 9, no. 2, pp. 600–608, May 2013, doi: 10.1109/TII.2012.2225433.

[16] D. Zhang, J. He, D. Pan, M. Dame, and M. Schutten, "Development of a high-power density megawatt-scale medium-voltage power converter for aircraft hybrid-electric propulsion systems," in *Proc. AIAA/IEEE Electr. Aircr. Technol. Symp. (EATS)*, Indianapolis, IN, USA, Aug. 2019, pp. 1–6, doi: 10.2514/6.2019-4472.

[17] S. Minaei, M. Yildiz, I. C. Göknar, and E. Yuce, "Negative impedance inverter and all-pass filter realizations using adder and subtractor blocks," in *Proc. IEEE 57th Int. Midwest Symp. Circuits Syst. (MWSCAS)*, College Station, TX, USA, Aug. 2014, pp. 567–570, doi: 10.1109/MWSCAS.2014.6908478.

[18] D. Rana, B. Hafez, P. Garg, S. Essakiappan, and P. Enjeti, "Analysis and design of active inductor as DC-link reactor for lightweight adjustable speed drive systems," in *Proc. IEEE Energy Convers. Congr. Expo. (ECCE)*, Sep. 2014, pp. 3243–3250.

[19] E. R. Ribeiro and I. Barbi, "Harmonic voltage reduction using a series active filter under different load conditions," *IEEE Trans. Power Electron.*, vol. 21, no. 5, pp. 1394–1402, Sep. 2006.

[20] J. Chen, X. Zhang, and C. Wen, "Harmonics attenuation and power factor correction of a more electric aircraft power grid using active power filter," *IEEE Trans. Ind. Electron.*, vol. 63, no. 12, pp. 7310–7319, Dec. 2016.

[21] J.-S. Lee and K.-H. Yu, "Optimal path planning of solar-powered UAV using gravitational potential energy," *IEEE Trans. Aerosp. Electron. Syst.*, vol. 53, no. 3, pp. 1442–1451, Jun. 2017.

[22] B. Lee, S. Kwon, P. Park, and K. Kim, "Active power management system for an unmanned aerial vehicle powered by solar cells, a fuel cell, and batteries," *IEEE Trans. Aerosp. Electron. Syst.*, vol. 50, no. 4, pp. 3167–3177, Oct. 2014, doi: 10.1109/TAES.2014.130468.

[23] G. de Carvalho Bertoli, G. M. Pacheco, and G. J. Adabo, "Extending flight endurance of electric unmanned aerial vehicles through photovoltaic system integration," in *Proc. Int. Conf. Renew. Energy Res. Appl. (ICRERA)*, Palermo, Italy, Nov. 2015, pp. 143–147, doi: 10.1109/ICRERA.2015.7418556.

[24] X. Zhu, Z. Guo, and Z. Hou, "Solar-powered airplanes: A historical perspective and future challenges," *Prog. Aerosp. Sci.*, vol. 71, pp. 36–53, Nov. 2014, doi: 10.1016/j.paerosci.2014.06.003.

[25] H. Wang and J. Shen, "Analysis of the characteristics of solar cell array based on MATLAB/simulink in solar unmanned aerial vehicle," *IEEE Access*, vol. 6, pp. 21195–21201, Apr. 2018, doi: 10.1109/ACCESS.2018.2802927.

[26] A. Kaplan, N. Kingry, P. Uhing, and R. Dai, "Time-optimal path planning with power schedules for a solar-powered ground robot," *IEEE Trans. Autom. Sci. Eng.*, vol. 14, no. 2, pp. 1235–1244, Apr. 2017, doi: 10.1109/TASE.2016.2533418.

[27] X. Wei, P. Yao, and Z. Xie, "Comprehensive optimization of energy storage and standoff tracking for solar-powered UAV," *IEEE Syst. J.*, vol. 14, no. 4, pp. 5133–5143, Dec. 2020, doi: 10.1109/JSYST.2020.2964579.

[28] T. E. Noll, J. M. Brown, M. E. Perez-Davis, S. D. Ishmael, G. C. Tiffany, and M. Gaier, "Investigation of the helios prototype aircraft mishap," NASA Langley Res. Center, NASA, Washington, DC, USA, Mishap Rep., Sep. 2004, vol. 1. [Online]. Available: http://www.nasa.gov/pdf/64317main_helios.pdf

[29] C. Roberts, M. Vaughan, and W. Bowman, "Development of a solar powered micro air vehicle," in *Proc. 40th AIAA Aerosp. Sci. Meeting Exhibit*, Jan. 2002, p. 703.

[30] H. Zhang, B. Kou, L. Zhang, and Y. Jin, "Digital controller design based on active damping method of capacitor current feedback for auxiliary resonant snubber inverter with LC filter," *Appl. Sci.*, vol. 6, no. 11, p. 377, Nov. 2016, doi: 10.3390/app6110377.

[31] S. A. Almohaimeed and M. Abdel-Akher, "Power quality issues and mitigation for electric grids with wind power penetration," *Appl. Sci.*, vol. 10, no. 24, p. 8852, Dec. 2020, doi: 10.3390/app10248852.

[32] S. Ghosh, D. Das, B. Singh, S. Janardhanan, and S. Mishra, "Frequency domain modeling of dual active bridge converter based on harmonic balance approach," *IEEE J. Emerg. Sel. Topics Ind. Electron.*, early access, Jan. 14, 2021, doi: 10.1109/JESTIE.2021.3051591.

[33] S. K. Dash and P. K. Ray, "A new PV-open-UPQC configuration for voltage sensitive loads utilizing novel adaptive controllers," *IEEE Trans. Ind. Informat.*, vol. 17, no. 1, pp. 421–429, Jan. 2021, doi: 10.1109/TII.2020.2986308.

[34] F. M. Alhuwaishel, A. S. Morsy, and P. N. Enjeti, "A new active output filter (AOF) for variable speed constant frequency (VSCF) power system in aerospace applications," *IEEE Trans. Power Electron.*, vol. 33, no. 2, pp. 1087–1093, Feb. 2018, doi: 10.1109/TPEL.2017.2682191.

[35] F. Alhuwaishel, N. A. Ahmed, and P. Enjeti, "Active output filter under nonlinear load condition for solar powered unmanned aircraft system," in *Proc. IEEE 6th Int. Conf. Renew. Energy Res. Appl. (ICRERA)*, San Diego, CA, USA, Nov. 2017, pp. 327–330, doi: 10.1109/ICRERA.2017.8191080.

[36] N. A. Ahmed, S. A. Rahman, and B. N. Alajmi, "Optimal controller tuning for P&O maximum power point tracking of PV systems using genetic and cuckoo search algorithms," *Int. Trans. Electr. Energy Syst.*, Sep. 2020, Art. no. e12624, doi: 10.1002/2050-7038.12624.

NABIL A. AHMED (Member, IEEE) received the B.Sc. and M.Sc. degrees in electrical engineering from the Electrical and Electronics Engineering Department, Assiut University, Egypt, in 1989 and 1994, respectively, and the Ph.D. degree in electrical engineering from the University of Toyama, Japan, in 2000. Since 1989, he has been with Assiut University, where he has been a Professor, since 2011. From October 2004 to April 2005, he was a Postdoctoral Fellow with the Electric Energy Saving Research Center, Kyungnam University, South Korea. From July 2005 to September 2006, he was a JSPS Postdoctoral Fellow with Sophia University, Japan. He is currently an Associate Professor with the Electrical Engineering Department, College of Technological Studies, The Public Authority of Applied Education and Training, Kuwait, on leave from Assiut University. His research interests include power electronics applications, variable speed drives, soft switching converters, and renewable energy systems and its integration to electric power grid. He is a member of the IEEE Industrial Electronics Society and the Institute of Electrical Engineering of Japan (IEEJ). He was a recipient of the Egypt State Encouraging of Research Prize 2005, the Japan Monbusho Scholarship 1996–2000, the JSPS Fellowship 2005–2007, the Best Paper Awards from ICEMS'05 and IATC'06 conferences, and the Best Presentation Award from ICEMS'04 conference. He listed in Marque's Who is Who in the World, since 2009.

FAHAD M. ALHUWAISHEL (Member, IEEE) received the B.E. degree in electrical engineering from Kuwait University, in 2010, and the M.Sc. and Ph.D. degrees in electrical engineering from Texas A&M University, in 2015 and 2021, respectively. He joined an internship program in Hyundai Engineering, Seoul, South Korea, in 2010. He joined an internship program with the Wireline Department, Shlumberger, Kuwait. He joined the Technology Improvement Department, EQUATE Petrochemical Company, as an Analyzer Engineer, Kuwait, in 2011. He joined the College of Technological Studies, The Public Authority for Applied Education and Training, Kuwait, in 2015, where he is currently an Assistant Professor. He is the holder of three U.S. patents. He has several publications within IEEE conferences/journals. He was honored to receive the prestigious Recognition Award by the Amir of Kuwait, in 2010. He was a recipient of the Golden Award from the Genève International Invention Expedition, in 2010. As well as he is a nationwide referee in the state of Kuwait for inventions category. He also served as a Reviewer for *IAS*, IEEE Journal of Emerging and Selected Topics in Power Electronics, and IEEE Transactions on Transportation Electrification journals.